SUPPORTING INFORMATION

TiO_2 Nanowire Photocatalyst for Dual-Ion Production in Laser Desorption/Ionization (LDI) Mass Spectrometry

Moon-Ju Kim[a], Jong-Min Park[a], Tae Gyeong Yun[a], Joo-Yoon Noh[a],

Min-Jung Kang[b], Jae-Chul Pyun[a,]*

[a]Department of Materials Science and Engineering, Yonsei University,

50 Yonsei-ro, Seodaemun-gu

Seoul, 03722, Republic of Korea.

Tel: +82 2 2123 5851 / Fax: +82 2 312 5375

[b]Korea Institute of Science and Technology (KIST), Seoul, Republic of Korea

*To whom correspondence should be addressed. Email: jcpyun@yonsei.ac.kr

Contents

1. Experimental section

Materials

The CHCA, DHB, and 9-AA (≥99.0% purity) were purchased from Sigma-Aldrich (St. Louis, MO, USA). Acetonitrile, sodium hydroxide, potassium hydroxide, and methylene blue were purchased from Sigma-Aldrich (St. Louis, MO, USA). The Ti plates (1 mm thick, ≥99.6% purity) were purchased from Goodfellow (Cambridge, England). The SiC abrasive papers (1200, 2400, and 4000 grit) were purchased from R&B Inc. (Daejeon, Korea). Valine, serine, glutamic acid, and histidine were purchased from Sigma-Aldrich (St. Louis, MO, USA). The TiO_2 nanoparticles (P25) were purchased from Evonik Industries AG (Essen, Germany). The oxalic, succinic, adipic, and suberic acids were purchased from Sigma-Aldrich (St. Louis, MO, USA). Deionized water was obtained using a Milli-Q® water purification system (Millipore, Billerica, MA, USA).

Synthesis of TiO_2 nanowires using the wet-corrosion method

The TiO_2 nanowires were prepared using a wet-corrosion process. Wet corrosion is one of the top–down methods and consists of the following three steps: (1) etching a Ti substrate with NaOH solution, (2) washing the substrate with water, and (3) thermal annealing of the substrate. First, the surface of a polished Ti plate ($30 \times 30 \times 1$ mm^3) was etched with a strong basic NaOH solution (10 M) for 24 h at room temperature under mild shaking. During the first step of the NaOH treatment, the TiO_6 units were distorted because the longer Ti-O bonds of the TiO_6 units were broken by the corrosive NaOH solution. Subsequently, Na^+ ions from the NaOH solution were positioned within the layer of broken pieces.[1] After the NaOH treatment, the Ti plate was thoroughly rinsed with deionized water to remove excess Na^+ ions and soaked in water for 48 h at room temperature under mild shaking. During the water treatment, the Na^+ ions intercalated between the distorted titanate layers were partially eliminated by the water. Lastly, to obtain a crystalline TiO_2 phase, the Ti plate was thermally annealed at 500 °C for 2 h in air.

Characterization of the TiO_2 nanowires obtained through wet corrosion

The surface morphology of the TiO_2 nanowires was characterized using field-emission scanning electron microscopy (FE-SEM) and a microscope purchased from JEOL (Tokyo, Japan). The thickness of the TiO_2 nanowire layer was analyzed using atomic force microscopy (AFM, Suwon, Korea) in non-contact mode. The crystal structure of the TiO_2 nanowires was characterized during each step of the wet-corrosion process using high-resolution X-ray diffraction (XRD, PANalytical diffractometer, Westborough, MA, USA) and a Cu-Kα X-ray source at 40 kV, 40 mA, a step rate of $2\theta = 3°$/min, and a glancing angle of $\theta = 1°$ against the incident beam. The surface state of the Ti plate was analyzed during each step of the wet-corrosion process using a Raman spectrometer (HORIBA Jobin-Yvon, Longjumeau, France) and Ar-ion laser with a wavelength of 514.5 nm and incident laser power of 0.5 mW. The diffuse reflectance of the synthesized TiO_2 nanowires was measured using a UV–visible (UV–Vis) spectrometer (PerkinElmer, Waltham, MA, USA) equipped with a diffuse reflectance measurement module. The optical band-gap energy was determined using the diffuse reflectance values transformed according to the Kubelka–Munk function. The surface characteristics of the TiO_2 nanowires were examined using a Fourier-transform infrared (FTIR) spectrometer (PerkinElmer, Waltham, MA, USA).

The relative photocatalytic activities of the synthesized TiO_2 nanowires were compared with that of TiO_2 nanoparticles (P25). The P25 solutions (final concentration of 10 and 100 μg/mL in deionized water, respectively; reaction volume of 2.5 mL) and synthesized TiO_2 nanowires (reaction area of 900 mm^2) were tested in terms of the photocatalytic oxidation of methylene blue. The methylene blue solutions (final concentration of 7 μg/mL in deionized water) with the TiO_2 nanostructures were irradiated using a continuous UV lamp with a wavelength of 365 nm (Vilber Lourmat, Marne-la-Vallee, France) to observe the color change from blue to colorless. The distance from the methylene blue solution with the TiO_2 nanowires and P25 solution to the UV lamp was set to 3 cm. The radiation intensity at this distance was calculated to be 8.78 mW/cm^2. The variation in the optical density of methylene blue was measured at a wavelength of 650 nm and monitored using a microplate reader

(Molecular Devices Co., San Jose, CA, USA).

LDI-TOF mass spectrometry of the solid TiO_2 nanowire matrix

The LDI-TOF mass spectrometry was performed using TiO_2 nanowires as solid matrix. Four types of dicarboxylic acids and four amino acids were dissolved in deionized water. The samples (1 μL, concentration range of 10–500 μg/mL) were dispensed onto the TiO_2 nanowire plate. Mass spectrometric analysis was performed using a Voyager DE-STR equipped with a N_2 laser (337 nm, AB Sciex, Foster City, CA, USA). The mass spectra were obtained in dual-ion mode using an accelerating voltage of 20 kV and second ion source voltage of 18 kV. The reflector voltage was set to 9.5 kV. The limit of detection (LOD) was estimated from the signal-to-noise (S/N) ratio. The S/N ratio of the mass spectra was calculated using the following equation:[2] $S/N = 2.5 \times (Signal - 0.5 \times Noise)/Noise$, where *Signal* represents the intensity of the mass peak at a certain m/z and *Noise* is the amplitude of the non-peak spectra, which was calculated to be three times the standard deviation (σ). The standard deviation of the non-peak spectra was estimated using a blank target and the same experimental setup. Based on this calculation, mass peaks with a S/N ratio larger than three were regarded to be signals and the corresponding concentration of the sample was considered to be the LOD.

\

2. Supporting table

TiO_2 photocatalyst	k_r (rate constant)
P25 with the amount of 25 µg	3.36×10^{-3} min^{-1}
P25 with the amount of 250 µg	1.53×10^{-2} min^{-1}
TiO_2-KOH with reaction area of 900 mm^2	7.46×10^{-3} min^{-1}
TiO_2-NaOH with reaction area of 900 mm^2	1.29×10^{-2} min^{-1}

Table S1. Kinetics of the photocatalytic degradation of methylene blue with TiO_2 nanoparticles (P25), TiO_2-KOH, and TiO_2-NaOH.

3. Supporting figures

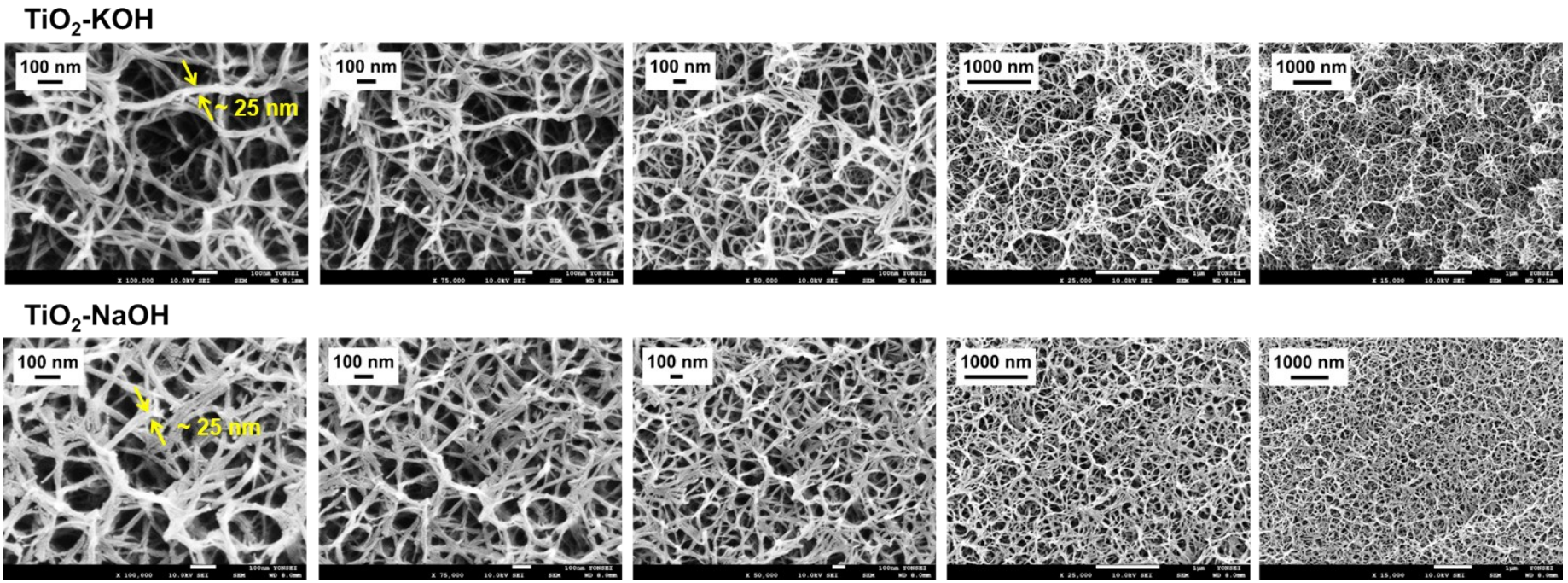

Figure S1. Surface morphology of randomly oriented TiO_2-KOH and TiO_2-NaOH. In TiO_2 nanowires obtained using KOH (TiO_2-KOH), aggregated parts were more frequently observed on the surface compared with those obtained using NaOH (TiO_2-NaOH). The morphologies of the TiO_2 nanowires were different since the corrosive power of KOH is higher than that of NaOH.[3]

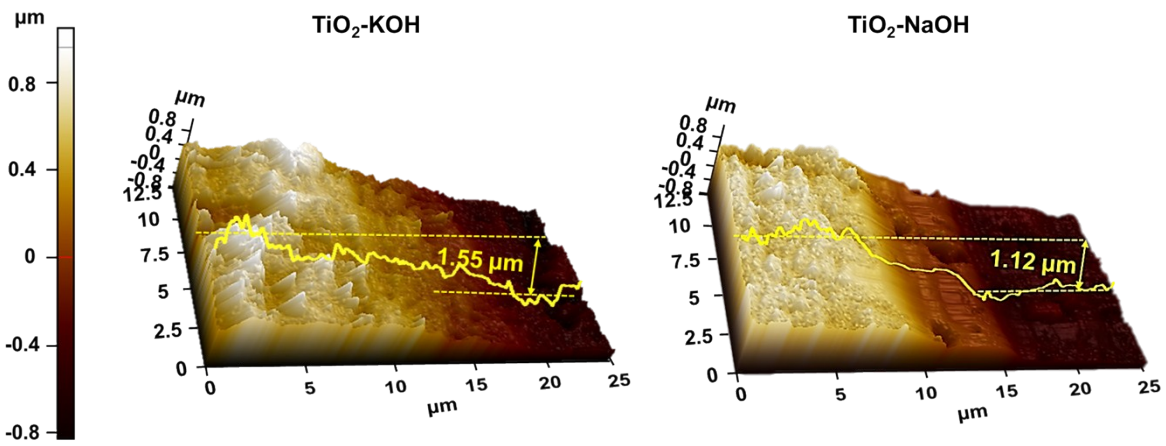

Figure S2. Thickness of the TiO_2-KOH and TiO_2-NaOH layers. The thicknesses of the TiO_2 nanowires were different since the corrosive power of KOH is higher than that of NaOH.[3]

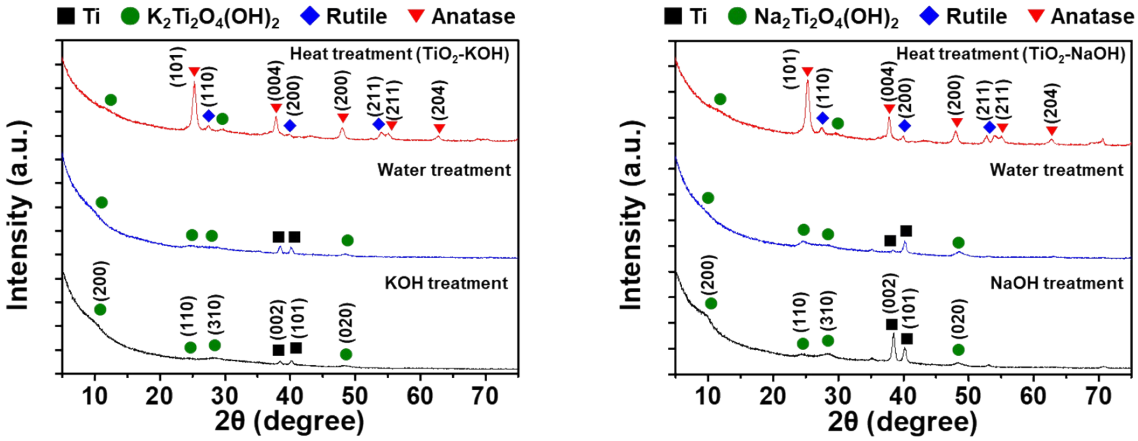

Figure S3. XRD patterns of the Ti substrate after each step of the wet-corrosion process. After the alkali and water treatments, Ti metal and titanate peaks can be observed in the XRD spectra of both of TiO_2-KOH and TiO_2-NaOH. After the final heat treatment, peaks of rutile and anatase phases as well as layered titanate can be observed in the XRD spectra. These results show that the two types of TiO_2 nanowires (TiO_2-KOH and TiO_2-NaOH) have similar crystal structures.

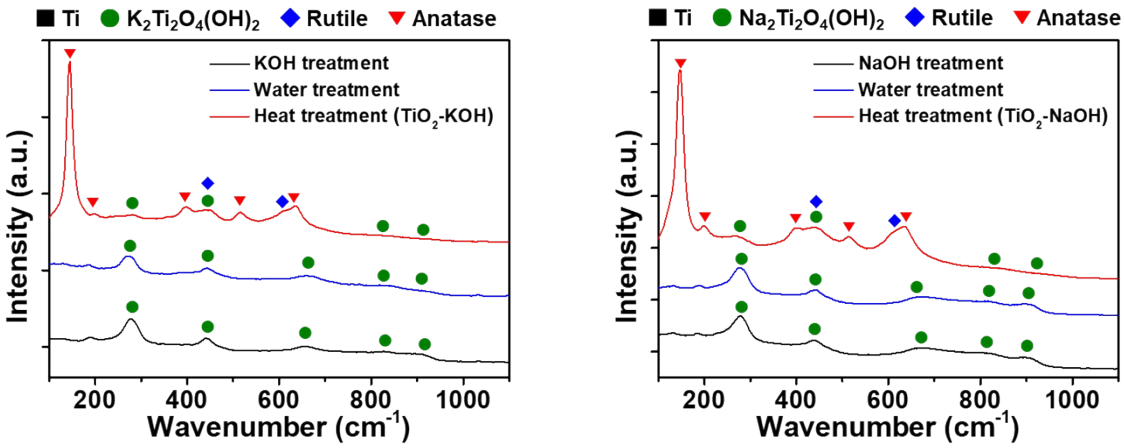

Figure S4. Raman spectra of the Ti substrate after each step of the wet-corrosion process. With XRD analysis, however, it was difficult to clarify the layered titanate phases, such as trititanate and lepidocrocite-type titanate. Among various compositions for the layered titanates synthesized with alkali solution (MOH) treatment, it was reported that two crystal structures of $M_2Ti_2O_4(OH)_2$ and $M_2Ti_3O_7$ were usually found in the layered titanate phases.[4,5] It is known that the degree of distortion of the TiO_6 unit is affected by the size, electronegativity of ions, amount of intercalated cations, and water, resulting in different basal spacings of the layered titanate phases.[6] Because the crystallinity of the titanate components of the TiO_2 nanowires obtained from the wet-corrosion process is too low to validate the crystal structure, micro-Raman analysis was performed. After the alkali and water treatments, the Raman band characteristic for the stretching vibration of short Ti-O terminal bonds of the distorted TiO_6 unit was observed in TiO_2-KOH and TiO_2-NaOH at 895 and 901 cm^{-1}, respectively. The crystal structures of TiO_2-NaOH and TiO_2-KOH were expected to contain the layered titanates $Na_2Ti_2O_4(OH)_2$ and $K_2Ti_2O_4(OH)_2$. These two crystal structures show no Raman peak at ~900 cm^{-1} because lepidocrocite-type titanates do not have terminal Ti-O bonds where the oxygen was unshared.[7] In addition, the Raman spectra of TiO_2-NaOH and TiO_2-KOH were distinctively different from those of trititanate in the range of 100–300 cm^{-1}, where trititnate shows complex spectral features.[6] After the heat treatment, the TiO_2 nanowires contained mixed phases of anatase and rutile and layered titanate.

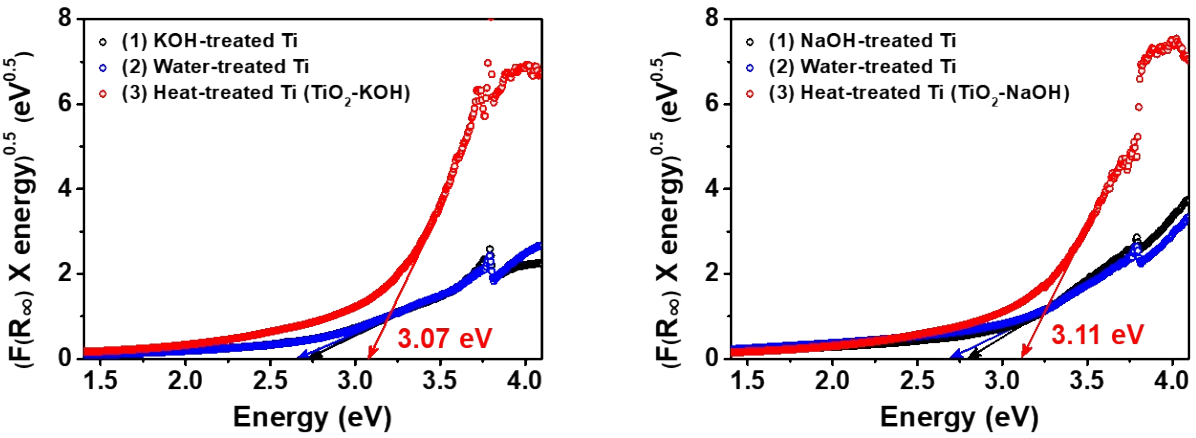

Figure S5. Tauc plots of $(F(R_\infty) \times h\nu)^{0.5}$ versus $h\nu$ for TiO_2 nanowires after each step of the wet-corrosion process. The diffuse reflectance (R_∞) of TiO_2-NaOH and TiO_2-KOH was measured with a UV–Vis spectrometer and the optical absorption coefficient [$F(R_\infty)$] was calculated from the reflectance data using the Kubelka–Munk method: $F(R_\infty) = (1 - R_\infty)^2/(2R_\infty)$.[8] The band-gap energy was evaluated via the extrapolation of the linear region in the Tauc plot [$(F(R_\infty) \times h\nu)^{0.5}$ versus $h\nu$]. Based on the calculation, the band gap of TiO_2-NaOH (and TiO_2-KOH) after the alkali, water, and heat treatments was estimated to be 2.79 (2.72), 2.68 (2.66), and 3.11 (3.07) eV, respectively. These results indicate that TiO_2-NaOH and TiO_2-KOH have similar band gaps.

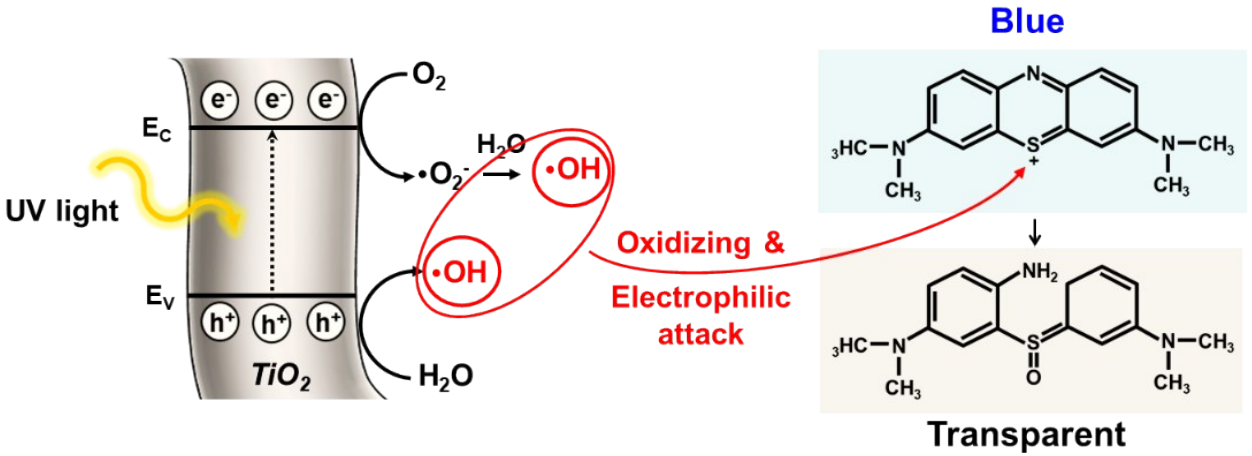

Figure S6. Photocatalytic degradation mechanism of methylene blue with TiO_2. The chromophoric group of methylene blue is oxidized by the attack of the hydroxyl radical under UV radiation. During the reorganization of the electrons, the sulfhydryl part ($C–S^+=C$) is converted to a sulfoxide [$C–(S=O)–C$] and the aromatic heterocycle in the center opens, thus, the color of methylene blue changes from blue to colorless.[9]

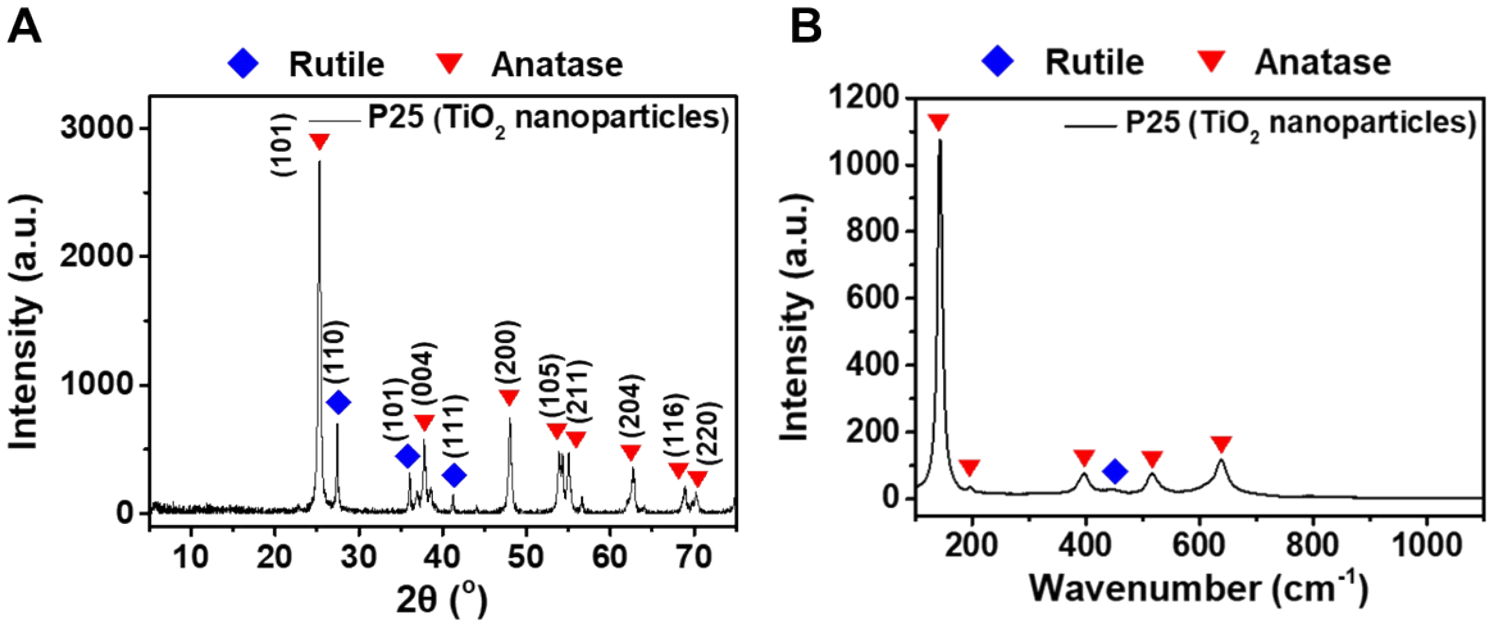

Figure S7. (A) XRD pattern of the TiO_2 nanoparticles (P25). (B) Raman spectrum of the TiO_2 nanoparticles (P25).

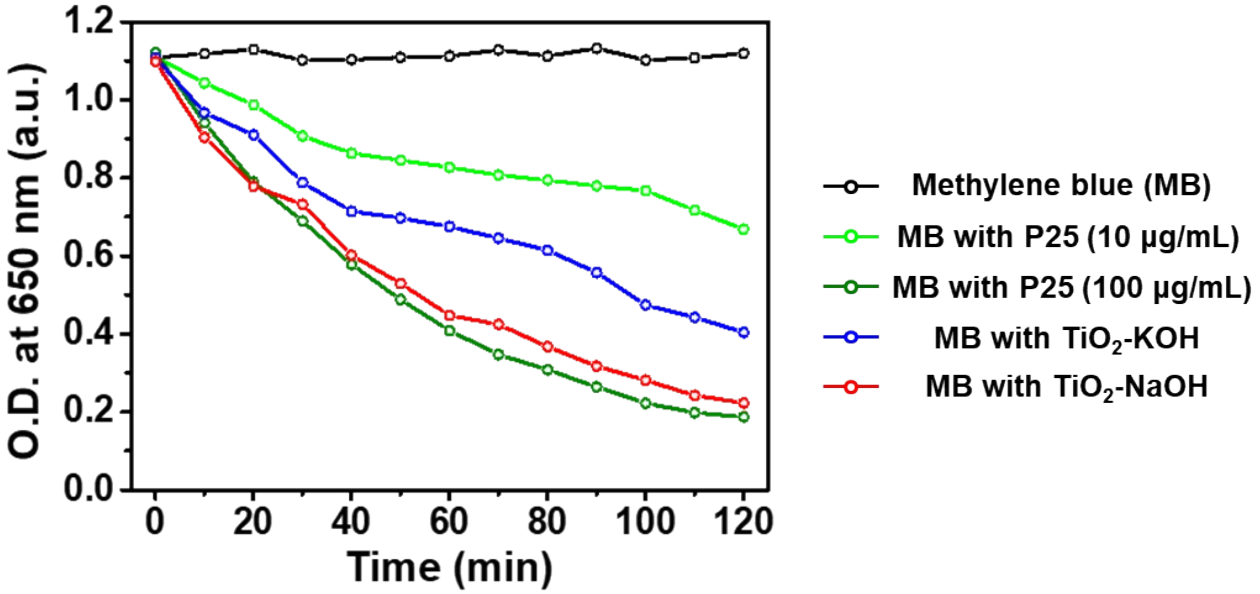

Figures S8. Comparison of the photocatalytic activities of the TiO_2 nanowires (TiO_2-KOH and TiO_2-NaOH) and TiO_2 nanoparticles (P25) based on the methylene blue degradation.

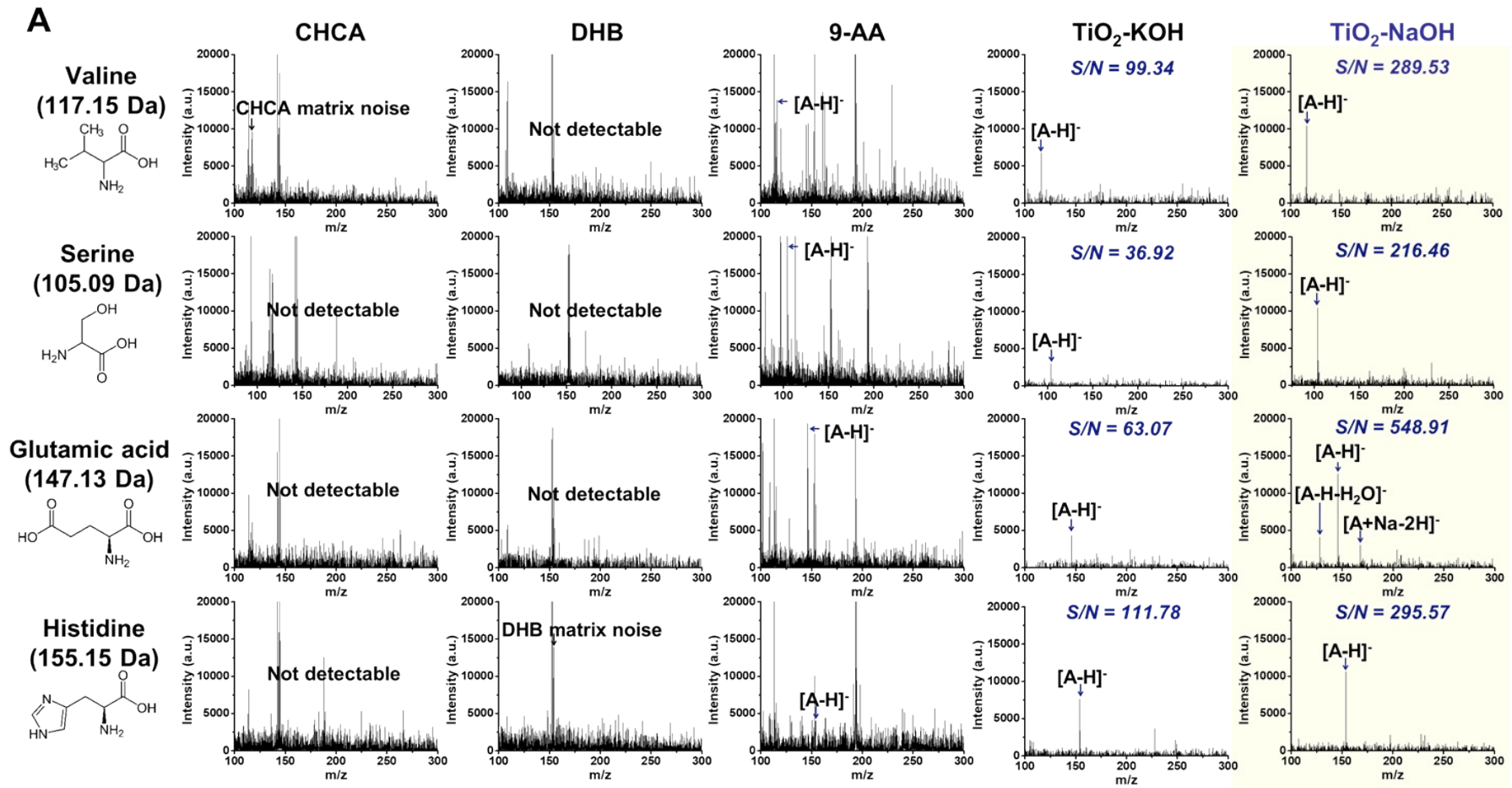

Figure S9. Comparison of the mass spectra of the four types of amino acids with organic matrices (CHCA, DHB, and 9-AA) and solid matrices (TiO_2–KOH and TiO_2–NaOH) in (A) negative ion mode, and (B) positive ion mode (continued).

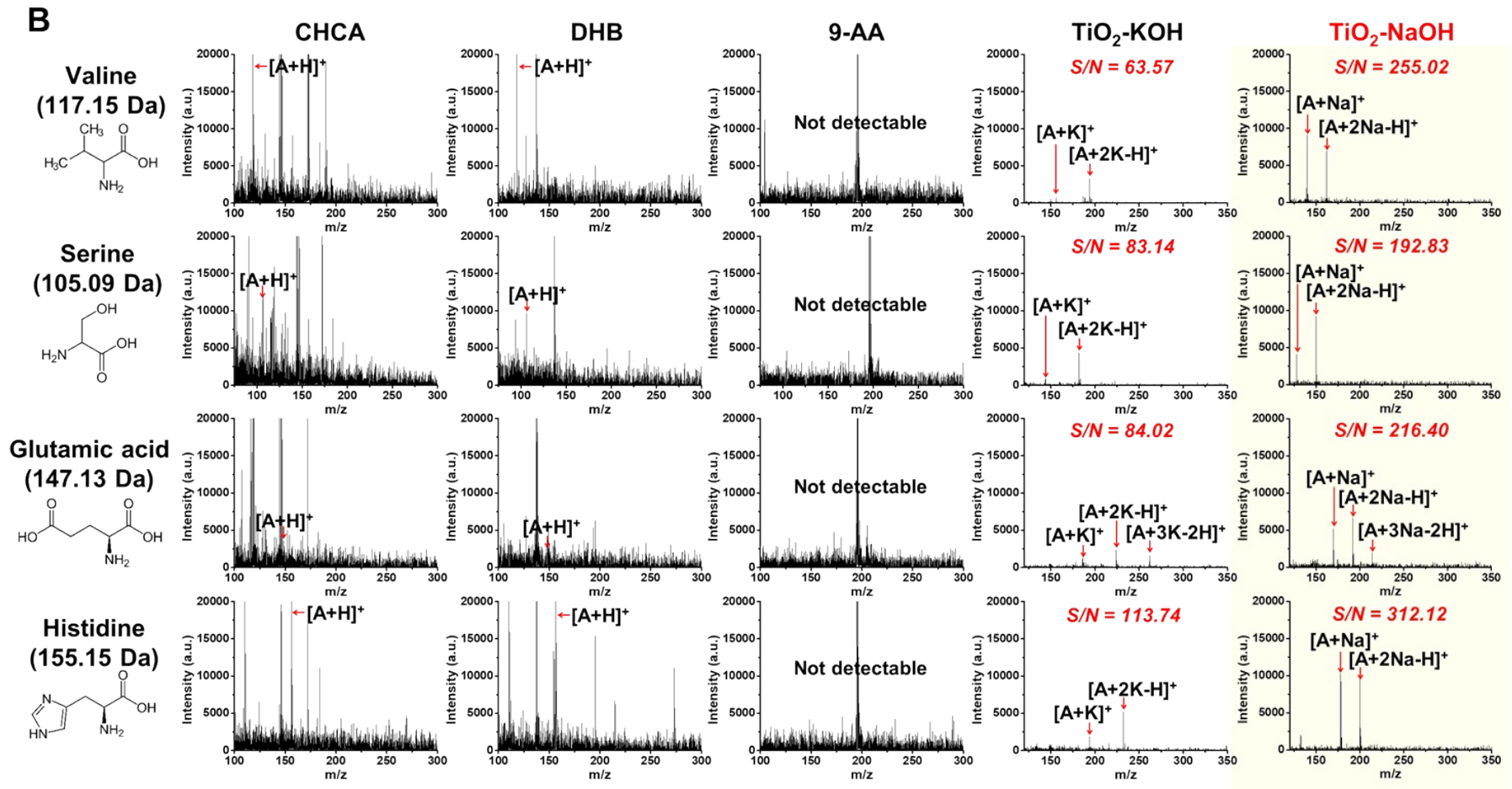

Figure S9. Comparison of the mass spectra of the four types of amino acids with organic matrices (CHCA, DHB, and 9-AA) and solid matrices (TiO_2–KOH and TiO_2–NaOH) in (A) negative ion mode, and (B) positive ion mode (continued).

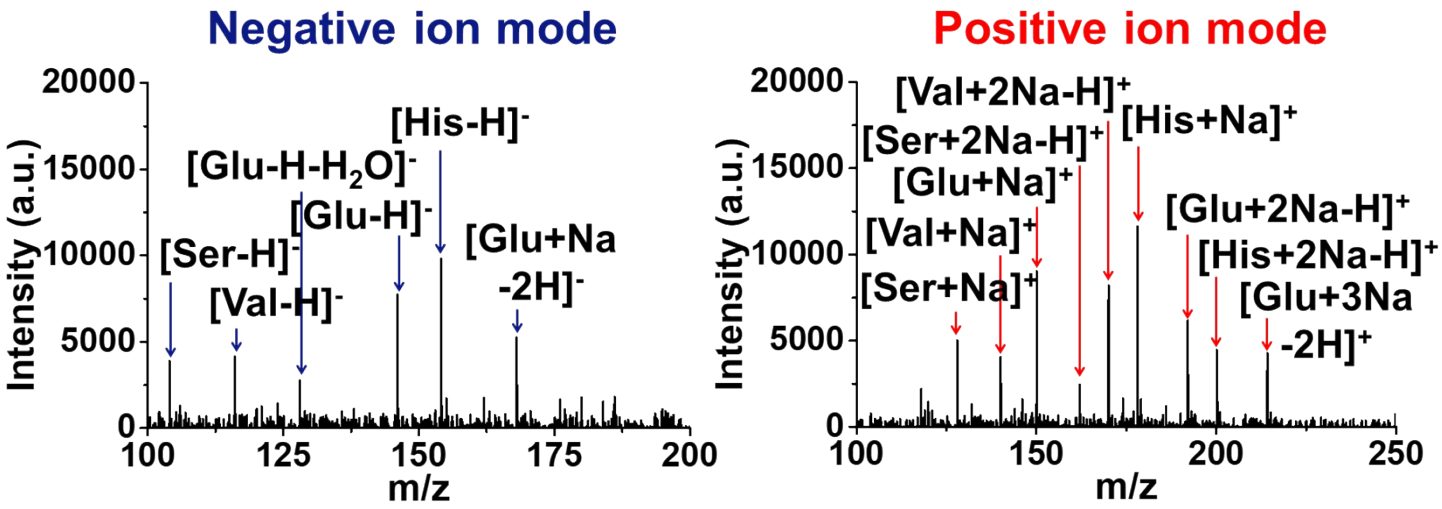

Figure S10. Simultaneous detection of the four amino acids with TiO_2 nanowires in negative ion mode, and positive ion mode.

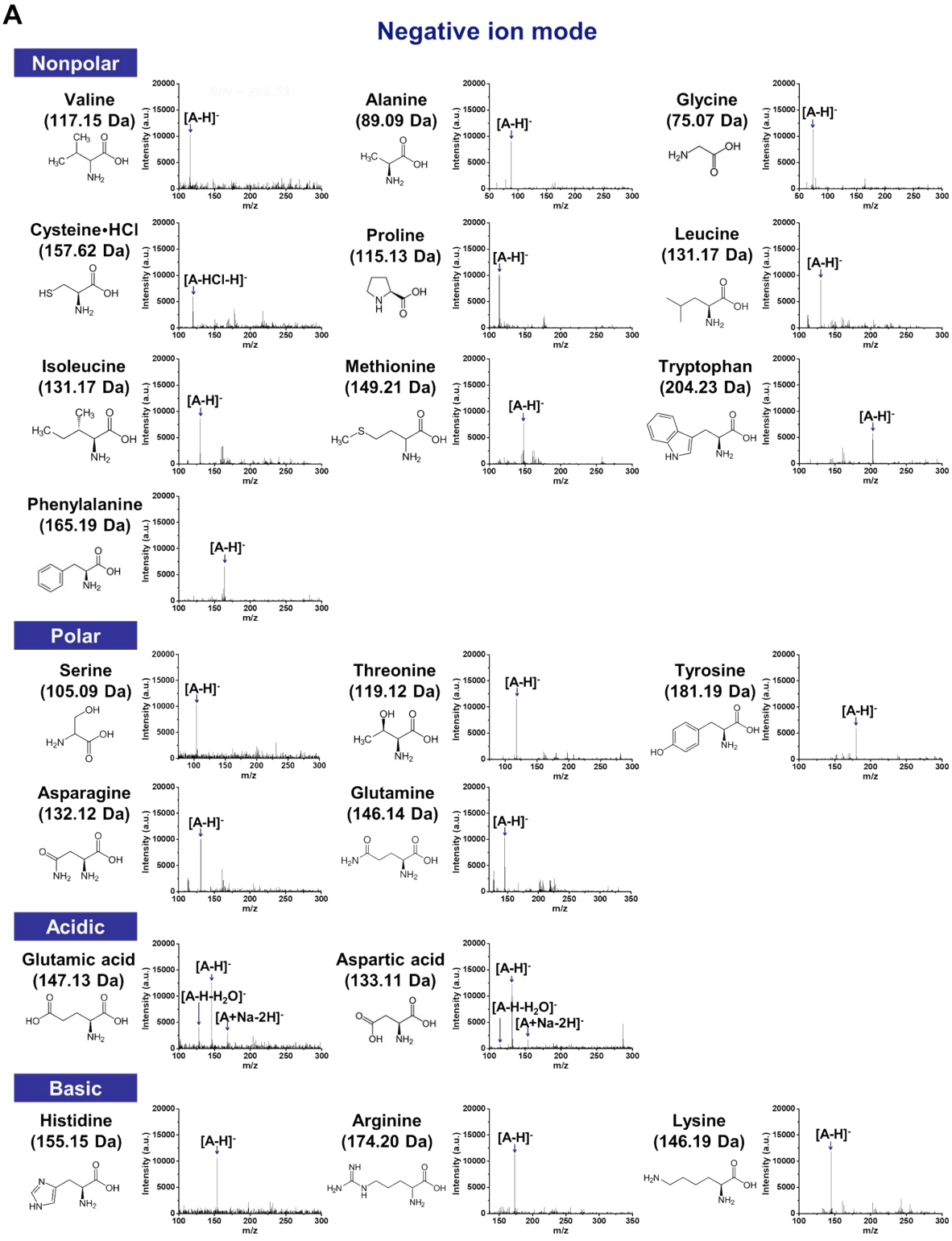

Figure S11. LDI-MS dual-ionization of essential amino acids (20 kinds) with TiO_2-NaOH solid matrix in (A) negative ion mode, and (B) positive ion mode (continued).

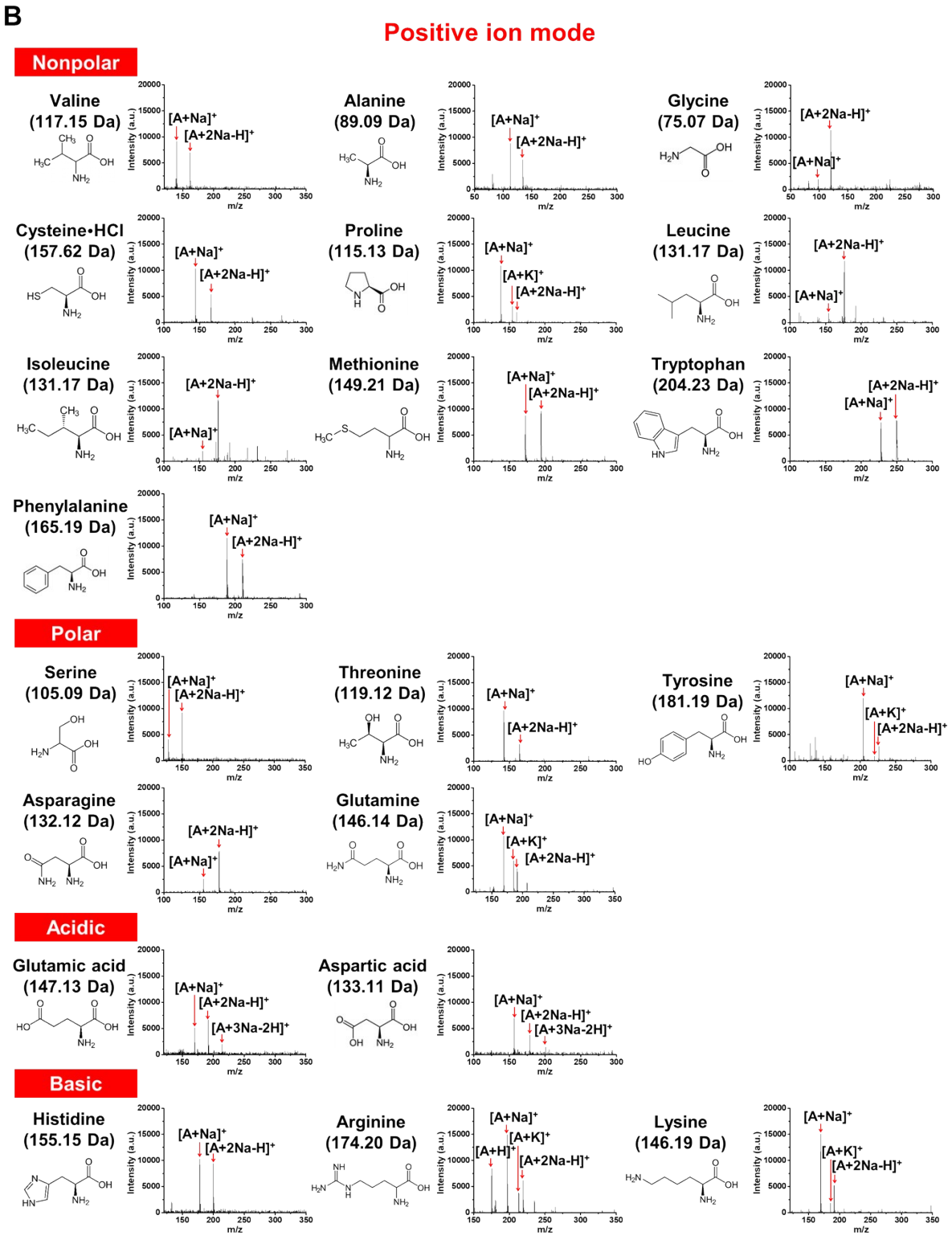

Figure S11. LDI-MS dual-ionization of essential amino acids (20 kinds) with TiO_2-NaOH solid matrix in (A) negative ion mode, and (B) positive ion mode (continued).

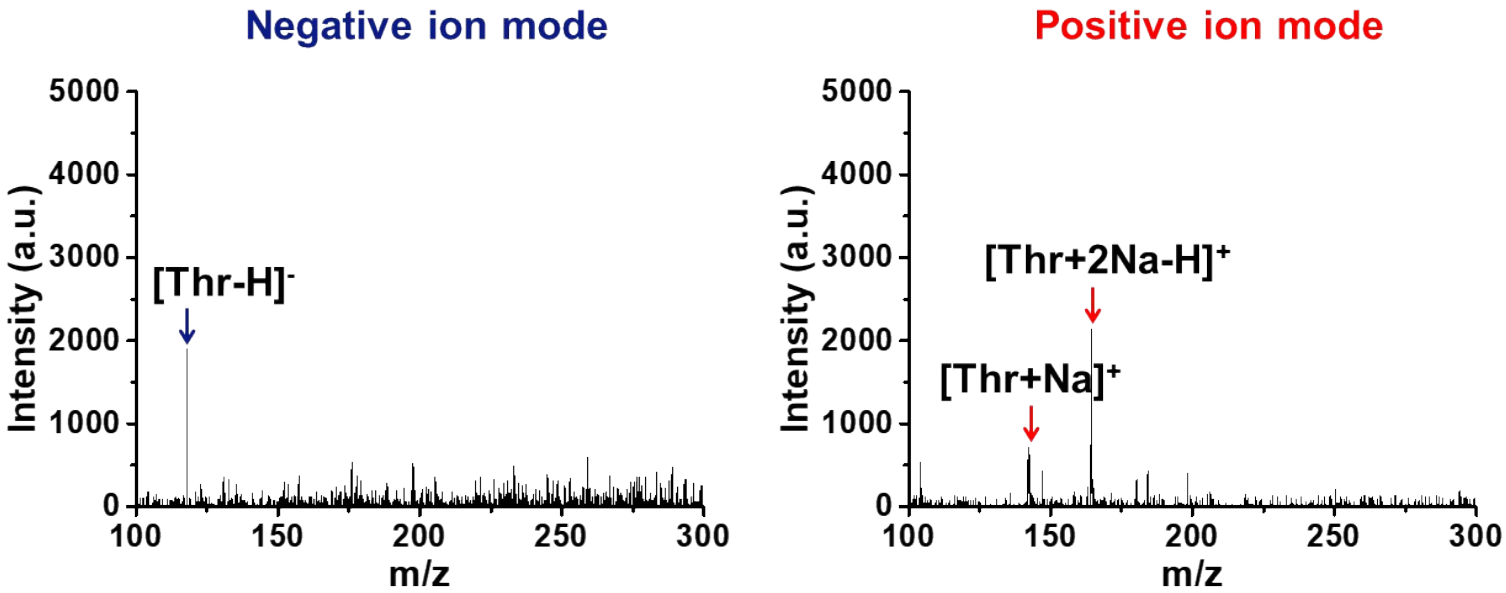

Figure S12. LDI-MS of threonine spiked in a serum sample after methanol-precipitation in negative and positive ion mode. The serum was spiked with threonine at the concentration of 250 μg/mL. In order to avoid noise peaks from the interference of various kinds of proteins for LDI-MS, methanol-precipitation was carried out by mixing threonine-spiked serum (10 μL) and cold methanol (90 μL).[10] And then, the mixture was centrifuged at 12000 rpm for 10 min and the supernatant was analyzed using LDI-MS. The final concentration of the threonine-spiked serum sample was determined to be 25 μg/mL after methanol treatment.

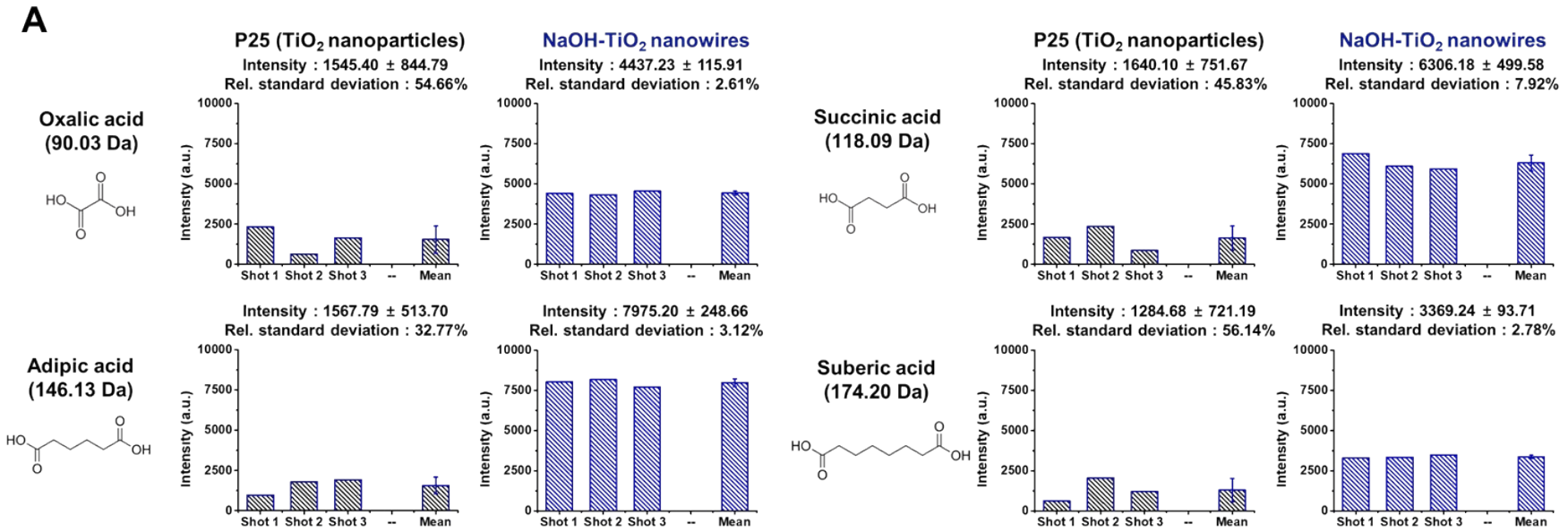

Figure S13. Comparison of the shot-to-shot reproducibility of P25 and TiO_2-NaOH using four dicarboxylic acids in (A) negative ion mode and (B) positive ion mode (continued).

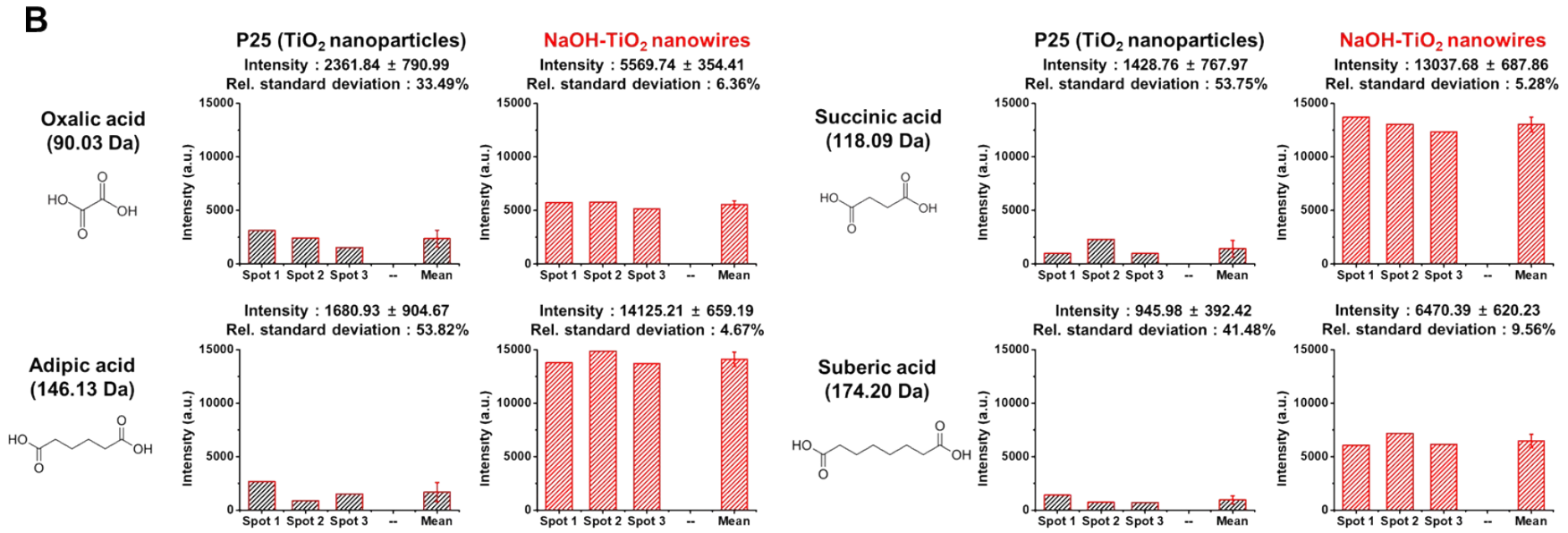

Figure S13. Comparison of the shot-to-shot reproducibility of P25 and TiO_2-NaOH using four dicarboxylic acids in (A) negative ion mode and (B) positive ion mode (continued).

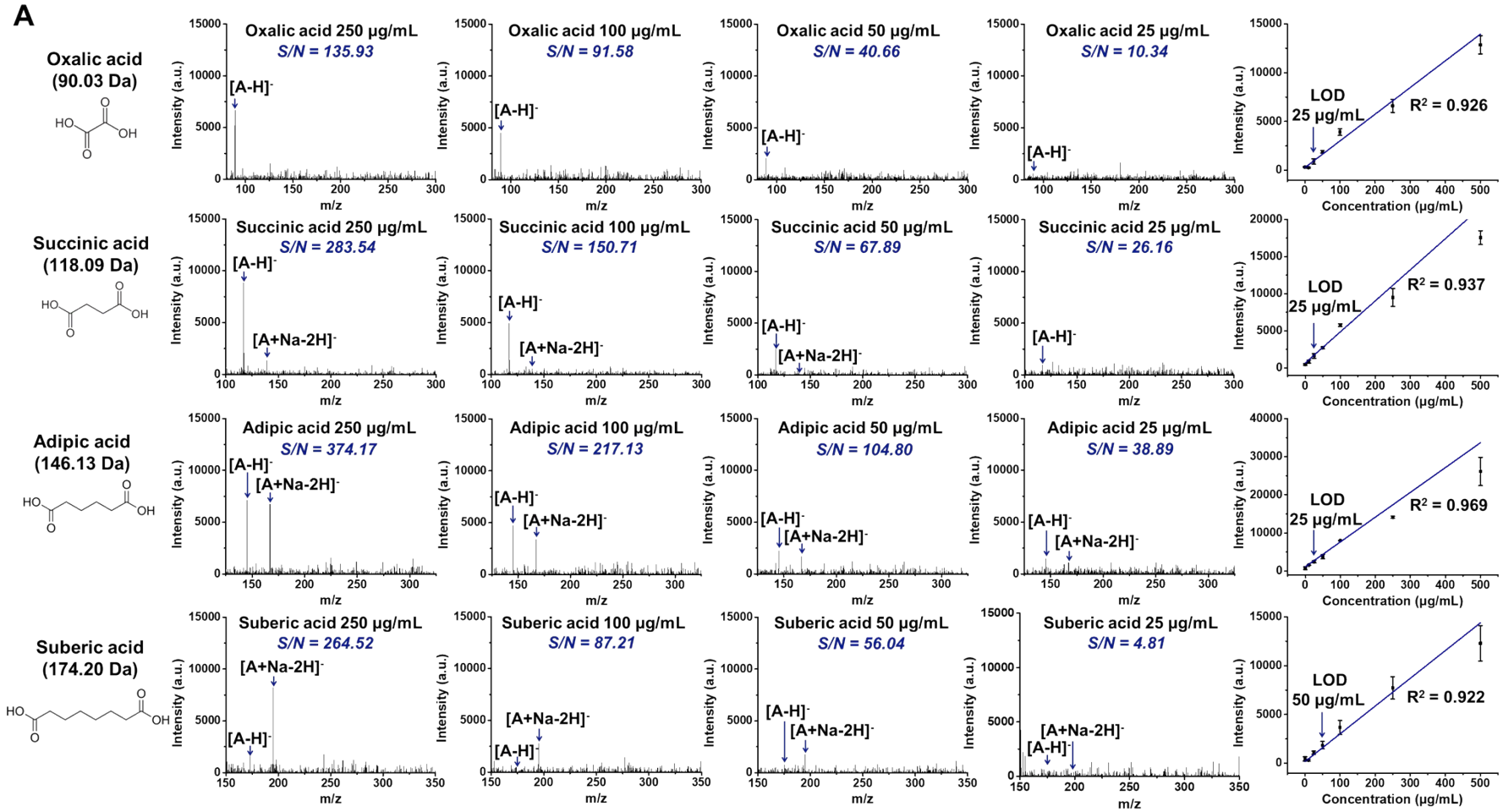

Figure S14. Quantification of the four dicarboxylic acids with high linearity using NaOH-TiO_2 in (A) negative ion mode, and (B) positive ion mode (continued)..

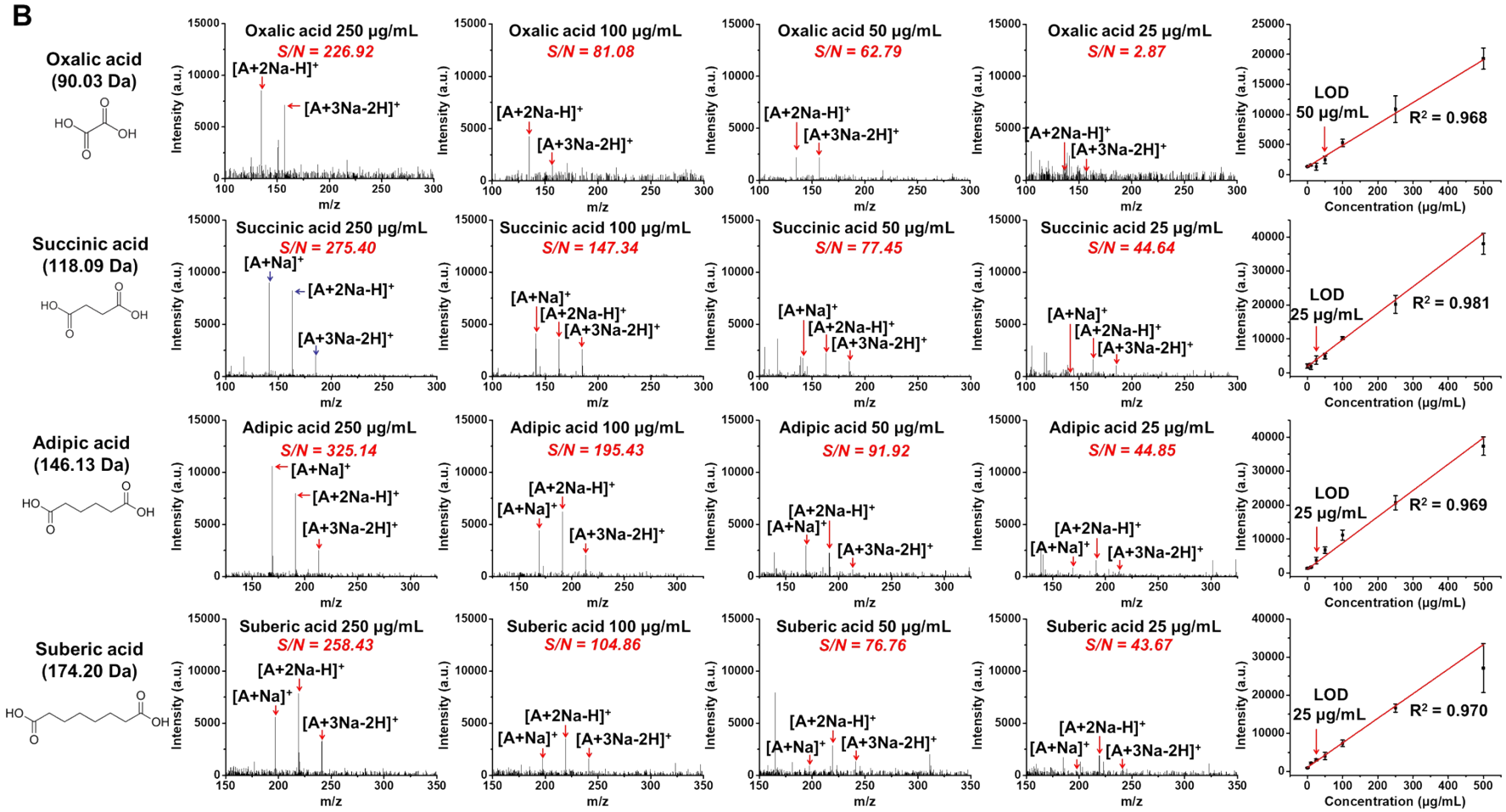

Figure S14. Quantification of the four dicarboxylic acids with high linearity using NaOH-TiO_2 in (A) negative ion mode, and (B) positive ion mode (continued).

References for SI

1 H.-H. Ou, S.-L. Lo, *Sep. Purif. Technol.*, 2007, **58**, 179-191.

2 S. Braun, H. Kalinowski, S.Berger, Wiley–VCH: Weinheim, Germany, 1998.

3 L. M. Sikhwivhilu, S. S. Ray, N. J. Coville, *Appl. Phys. A*, 2009, **94**, 963-973.

4 D. V. Bavykin, J. M. Friedrich, F. C. Walsh, *Adv. Mater.*, 2006, **18**, 2807-2824.

5 M. J Li, Z. Y. Chi, Y. C. Wu, *J. Am. Ceram. Soc.*, 2012, **95**, 3297-3304.

6 M. Kim, J.-M.; Park, T. G. Yun, J.-Y. Noh, M.-J. Kang, J.-C. Pyun, *ACS Appl. Mater. Inter.*, 2018, **10**, 33790-33802.

7 B. C. Viana, O. P. Ferreira, A. G. Souza Filho, A. A. Hidalgo, J. Mendes Filho, O. L. Alves, *Vib. Spectrosc*., 2011, **55**, 183-187.

8 H. Lin, C. Huang, W. Li, C. Ni, S. I. Shah, Y.-H. Tseng, *Appl. Catal. B. Environ.*, 2006, **68**, 1-11.

9 C. Yang, W. Dong, G. Cui, Y. Zhao, X. Shi, X. Xia, B. Tang, W. Wang, *RSC Adv.*, 2017, **7**, 23699-23708.

10 J.I. Kim, S.Y. Ryu, J.M. Park, J.Y. Noh, M.J. Kang, S.Y. Kwak, J.C. Pyun, *Rapid Commun. Mass Spectrom.*, 2014, **28**, 2427-2436.